JOURNAL OF GUIDANCE, CONTROL, AND DYNAMICS
Vol. 26, No. 5, September–October 2003

Optimal Update Scheme for Drag Reference Profiles in an Entry Guidance

W. Grimm* and J. G. van der Meulen†
University of Stuttgart, 70550 Stuttgart, Germany
and
A. J. Roenneke‡
Astrium, 28361 Bremen, Germany

Entry guidance with an optimal update scheme for the drag reference profile is presented. The guidance is designed for entry in the neighborhood of a specified nominal flight path. To account for off-nominal conditions, the nominal flight path is modified onboard to obtain a reference trajectory for the subsequent guidance cycle. The reference trajectory is adapted to the actual position and velocity. In particular, it provides the range required to reach the target. The reference trajectory is defined as the solution of a variational problem with the objective to stay as close as possible to the nominal entry path. With an appropriate representation of the reference trajectory, the variational problem reduces to an unconstrained quadratic program. This allows for a direct, closed-form solution suitable for onboard application. Rigid-body simulations with model perturbations and modified entry conditions demonstrate the performance of the guidance.

Nomenclature

D	=	drag force
e	=	specific energy
$f(e)$	=	weight-to-drag ratio, $W_{\text{sea}}/D(e)$
g	=	gravitational acceleration
h	=	altitude
$\boldsymbol{M}$	=	moment vector of a cubic spline function
m	=	vehicle mass
R_{Earth}	=	radius of Earth
s	=	range to target along ground track
V	=	velocity (Earth relative)
W	=	weight
$w(e)$	=	weighting function
$\boldsymbol{y}$	=	array of function values of a cubic spline function

Subscripts

f	=	final value, value at the target point
ini	=	value at the beginning of a trajectory update cycle
nom	=	value of the nominal trajectory
ref	=	value of the reference trajectory
sea	=	value at sea level, for example, g_{sea}, W_{sea}

Superscript

$'$	=	differentiation with respect to energy

I. Introduction

THE entry guidance of the space shuttle[1] provides the basic scheme for most of the entry guidance methods that are discussed today. The first step is to design a nominal trajectory before the actual mission, which is stored as a drag profile in the guidance software. For range control, the nominal drag profile is modified onboard. The onboard update will be called reference trajectory in the sequel. The entry vehicle follows the reference trajectory with a drag tracking controller, which determines the magnitude of the commanded bank angle. The sign of the bank angle is determined to reduce the lateral target miss.

The contribution of the present paper is an online optimization scheme for shaping the reference trajectory. Therefore, the paper focuses on this component of the entry guidance. The space shuttle guidance[1] provides nonlinear, analytical formulas for the onboard computation of the reference trajectory. Another way to define the reference trajectory is a uniform scaling of the nominal drag profile to obtain the required range to the target.[2] Lu[3] and Lu and Hanson[4] represent the reference trajectory as a piecewise linear drag-vs-energy profile. The entry-path constraints (heat flux, load factor, and dynamic pressure constraints) can be regarded as bounds on the drag profile. Therefore, they can be incorporated in the optimization process for the drag reference profile.[3,4] Several authors propose online trajectory planning by using different methods for real-time integration and optimization with explicit consideration of path constraints.[5–8] This allows for an online computation of the nominal trajectory supposing a high-performance onboard computer. Dukeman[9] shows that range control can also be performed with linear control theory. To this end, the range-to-go is included as a state variable in a control design model and tracked with a linear quadratic regulator controller.

The present guidance scheme is based on concepts of Roenneke.[10] Roenneke[10] uses a variational approach to update the reference trajectory in the form of drag vs energy. It is optimal in the sense that it maximizes the ranging authority within the entry corridor. Additionally, it starts at the actual vehicle state and provides the required range-to-go. The resulting variational problem is reduced to a nonlinear program via discretization and is iteratively solved onboard. The main contribution of the present paper is as follows. Under certain technical restrictions, the nonlinear program for the reference trajectory reduces to an unconstrained quadratic program. This allows for a direct solution without any iterative procedures and, thus, avoids the usual problems of real-time optimization: computational effort and reliable convergence.

To complete the guidance algorithm, the reference trajectory generator is combined with nonlinear drag tracking control[2,11,12] and a traditional bank reversal logic.[1] A departure of a capsule-type

Received 1 August 2002; revision received 24 March 2003; accepted for publication 25 March 2003.

*Research Scientist, Institute of Flight Mechanics and Control, Pfaffenwaldring 7a; werner.grimm@ifr.uni-stuttgart.de.

†Research Scientist, Institute of Flight Mechanics and Control, Pfaffenwaldring 7a; jaap.vandermeulen@stork.com.

‡Head of Reusable Launch Vehicle Programs, Space Infrastructure; axel.roenneke@astrium-space.com. Senior Member AIAA.

vehicle from the International Space Station (ISS) orbit to Captieux, France, serves as the test case. The nominal entry flight has been computed with the trajectory optimization software ASTOS.[13] The associated drag-vs-energy profile plays the role of the nominal trajectory. The performance of the guidance is verified in six-degrees-of-freedom simulations over an oblate Earth. Preliminary results have been published in previous papers.[14,15]

II. Vehicle Model and Reference Mission

The reference mission is an entry flight from the circular ISS orbit (400-km altitude, 51.58-deg inclination) to Captieux, France (44.4° N, 0.4° W). The reference vehicle is a small, unmanned capsule with a lift-to-drag ratio of approximately 0.4 (Table 1). For attitude control during entry, a reaction control system (RCS) of four thrusters, each with a maximum thrust of 10 N, is used, resulting in a control torque of approximately 4–7 N · m per axis.[16] Because of the limited aerodynamic performance of the vehicle, the accessible landing area from nominal entry conditions is about 1000 km downrange and 150 km crossrange.[16]

The simulation of the guided entry flight phase starts at the perimeter of the atmosphere at 120-km altitude and is terminated at the drogue chute release conditions at 25-km altitude and approximately Mach 1.5. In the next flight phase, target approach and landing is performed by means of a controllable parafoil system.[14,15]

To compute the reference mission, the so-called entry corridor is defined as follows. The heat flux and acceleration limit represent the upper boundaries, the lower boundary is given by the equilibrium glide path (Fig. 1). The equilibrium glide-path constraint represents a controllability limit and is computed with a bank angle margin of 30 deg during hypersonic flight. With the entry corridor defined, the nominal flight path is an optimal trajectory in the following sense. The objective is to keep the nominal drag-vs-velocity profile as close as possible to the centerline of the entry corridor. This is a first approach to get a nominal trajectory with a sufficient margin to all

Table 1 Model constants of the entry vehicle

Variable	Value
Mass	100 kg
Lift-to-drag ratio	0.38
Maximum permitted heat flux	1.2 MJ/m^2
Maximum permitted acceleration	5 g
I_{xx}	6.08 kg · m^2
I_{yy}	11.39 kg · m^2
I_{zz}	9.98 kg · m^2
$I_{xz} = I_{zx}$	−3.28 kg · m^2
Maximum RCS torque in x direction	5.7N · m
Maximum RCS torque in y direction	4.4N · m
Maximum RCS torque in z direction	3.8N · m

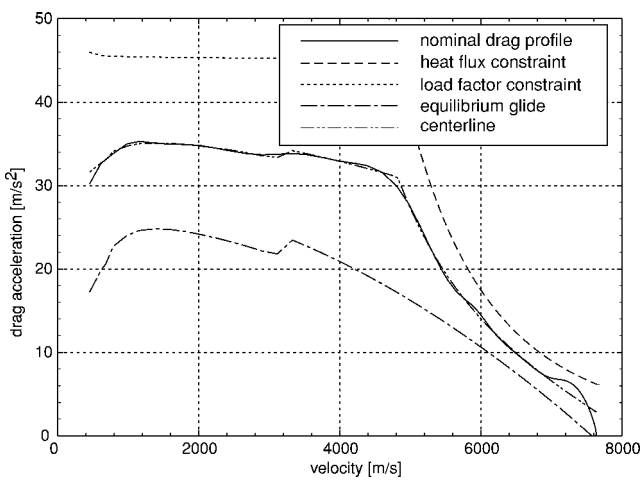

Fig. 1 Nominal trajectory and entry corridor in the drag acceleration vs velocity diagram.

Table 2 Variation of the entry conditions due to the variation of the deorbit impulse

Quantity	Cases 1, 2, and 5 (nominal)	Case 3 ($\Delta V = -2$ m/s)	Case 4 ($\Delta V = +2$ m/s)
Declination, deg	50.5766	50.8960	50.2713
Longitude, deg	−52.2374	−49.9413	−54.4313
Altitude, km	120	120	120
Velocity, m/s	7602.19	7604.10	7600.28
Flight-path angle, deg	−1.5778	−1.5303	−1.6240
Heading angle, deg	77.6434	77.6434	77.6434

path constraints. In case of small disturbances, the path constraints will not be violated. The optimal control problem for the nominal trajectory is solved by use of the software package ASTOS.[13]

In the optimization, the deorbit phase is modeled as an impulsive maneuver followed by a Keplerian arc. This allows the optimization of the following deorbit parameters: the magnitude of the deorbit impulse, the longitude of the ascending node of the ISS orbit, and the true anomly. The resulting entry conditions are shown in Table 2.

Figure 1 shows the optimal entry trajectory in the drag-vs-velocity plane. After an initial transition, it follows closely the centerline of the entry corridor as desired by the chosen optimization criterion.

III. Guidance Algorithm

The optimal trajectory shown in Fig. 1 is used as the nominal trajectory for the guidance design. The onboard guidance strategy is to compute the reference trajectory command by adapting the nominal trajectory to off-nominal conditions in target range, aerodynamic performance, or atmospheric dispersions. The reference trajectory is computed so that it is as close as possible to the nominal trajectory subject to the constraint that it covers the required range to the target and accounts for the current vehicle state. The reference trajectory is represented as a drag-vs-energy profile and is updated regularly onboard. To track the reference trajectory command, a nonlinear path controller is used based on nonlinear dynamic inversion.[2,11,12] The controller output is the absolute value $|\mu|$ of the bank angle. A conventional bank reversal logic[1] determines the sign of μ to counteract the lateral target miss with a specified deadband. The task of the attitude controller is to adjust the actual bank angle to the guidance command. The attitude controller used in the simulations is taken from Ref. 17 and has been configured for the capsule.

A. Range Estimate Based on the Drag Profile

The reference trajectory is represented as a drag-vs-energy profile. This is an established approach on the design of entry guidance.[2–5,10,11,18] Let e be specific energy defined as follows:

$$e = [V^2/(2 \cdot g_{\text{sea}})] + [R_{\text{Earth}}/(R_{\text{Earth}} + h)] \cdot h \tag{1}$$

The specific energy has units of length and is also referred to as energy height.[5] Def. (1) correlates with an inverse-square model of gravity for a spherical Earth given as

$$g = g_{\text{sea}} \cdot [R_{\text{Earth}}/(R_{\text{Earth}} + h)]^2 \tag{2}$$

For flight over a spherical, nonrotating Earth, the energy rate of change becomes[10,11]

$$\dot{e} = [V \cdot D/(m \cdot g_{\text{sea}})] \tag{3}$$

Given the drag-vs-energy profile, the range s to the target along the ground track can be estimated as[3,11]

$$s = \int_{e_f}^{e_{\text{ini}}} \frac{m \cdot g_{\text{sea}}}{D}\,\mathrm{d}e = \int_{e_f}^{e_{\text{ini}}} \frac{W_{\text{sea}}}{D}\,\mathrm{d}e \tag{4}$$

where the subscript ini refers to the current state, which represents the initial state of the remaining flight and thus the initial condition of the reference trajectory and subscript f denotes the end of the hypersonic entry phase.

B. Variational Problem for the Reference Trajectory

The reference trajectory command calculated by the onboard guidance is a direct solution of a variational trajectory optimization problem[10] as detailed as follows. Define the nominal and the reference trajectories as a function of W_{sea}/D vs e:

$$f_{ref}(e) = W_{sea}/D_{ref}(e), \qquad f_{nom}(e) = W_{sea}/D_{nom}(e)$$

$$\Delta f(e) = f_{ref}(e) - f_{nom}(e) \tag{5}$$

The performance criterion for the onboard optimization is chosen to minimize the deviation from the nominal trajectory[10]

$$I[f_{ref}] = \int_{e_f}^{e_{ini}} \frac{\Delta f(e)^2}{w(e)} \cdot de \tag{6}$$

subject to boundary conditions to be detailed. The integrand in Eq. (6) represents a penalty term for the deviation from the nominal trajectory in a least-square sense, and w is a positive weighting function, the selection of which is explained in the next section. Because the reference trajectory shall be smooth and nonoscillating, an additional penalty term is introduced to restrict the curvature of the reference trajectory. $\Delta \boldsymbol{M}$ is an array of $\Delta f''$ values taken at specified energy nodes (see next section). $\boldsymbol{C}$ is a positive definite matrix. Thus,

$$I[f_{ref}] = \int_{e_f}^{e_{ini}} \frac{\Delta f(e)^2}{w(e)} \cdot de + \frac{1}{2} \cdot \Delta \boldsymbol{M}^T \boldsymbol{C} \Delta \boldsymbol{M} \tag{7}$$

It is sufficient to select $\boldsymbol{C}$ to be a multiple of the unity matrix. The penalty term in Eq. (7) resembles the regularization technique in Refs. 3 and 4. Performance index (7) is minimized subject to the following boundary conditions, as shown in Ref. 10:

1) The initial conditions of the reference trajectory, e_{ini}, $f_{ref}(e_{ini})$, and $f'_{ref}(e_{ini})$ correspond to the actual values of the vehicle at the time the guidance algorithm is called. The values are derived from measurements.

2) The terminal point of the reference trajectory, e_f and $f_{ref}(e_f)$, correspond to the desired terminal state of the vehicle ($V_f = 450$ m/s and $h_f = 25$ km).

3) Also $f_{ref}(e)$ satifies the range matching condition (4).

Item 1 is a refinement compared to the shuttle guidance. Because the reference trajectory accounts for the current state there is a smooth transition onto the commanded drag profile instead of a sudden jump.

The parameter $f'_{ref}(c_{ini})$ involves the drag rate $\dot{D}$. $\dot{D}$ is estimated using a closed-form expression that assumes a constant drag coefficient and a locally exponential atmosphere, simplifications, which are established since the design of the shuttle guidance.[1]

The guidance does not explicitly account for path constraints such as heating, dynamic pressure, or load factor constraints. Rather, it relies on the margin along the nominal trajectory. Because the performance index (7) minimizes the deviation from the nominal trajectory, violation of the path constraints occurs in extremely off-nominal situations, only. All path constraints can be represented as lower and upper bounds in the drag-vs-energy plot. Therefore, they could be incorporated in the preceding formulation by adding upper and lower bounds on $f_{ref}(e)$.

C. Spline Approximation of the Reference Trajectory

Numerically, $f_{ref}(e)$, $f_{nom}(e)$, and $\Delta f(e)$ are represented as cubic splines over a partition,

$$e_f = e_0 < e_1 < \cdots < e_n = e_{ini} \tag{8}$$

of the energy interval $[e_f, e_{ini}]$ to be covered on the remaining flight. The lower bound e_f is the specified terminal energy, and the upper bound e_{ini} is the energy value at the moment the guidance algorithm is called. Cubic splines are known for undesired oscillations. They are damped by the penalty term on the curvature in the augmented performance index (7).

The parameters $f_{ref}(e)$, $f_{nom}(e)$, and $\Delta f(e)$ are essentially determined by their values at the nodes (8):

$$f_{ref}(e_i) = y_{ref,i}, \qquad f_{nom}(e_i) = y_{nom,i}$$

$$\Delta f(e_i) = \Delta y_i = y_{ref,i} - y_{nom,i} \tag{9}$$

The data $y_{nom,i}$ are taken from the nominal trajectory data set. Therefore, they represent known inputs to optimization problem (7), which is to be solved for the parameters $y_{ref,i}$.

In between each two nodes of partition (8), the cubic splines are cubic polynomials, whose coefficients do not only require the function values (9) but also second derivatives such as

$$\boldsymbol{M}_{ref} = (M_{ref,0}, \ldots, M_{ref,n})^T$$

with $M_{ref,i} = f''_{ref}(e_i)$. Similarly, the array $\boldsymbol{M}_{nom}$ of the nominal trajectory is defined, and the difference

$$\Delta \boldsymbol{M} = \boldsymbol{M}_{ref} - \boldsymbol{M}_{nom} \tag{10}$$

contains the second derivatives of $\Delta f(e)$. $\Delta \boldsymbol{M}$ is just the vector that defines the penalty term on the curvature in Eq. (7).

The nominal trajectory is defined as a natural cubic spline characterized by the properties

$$M_{nom,0} = M_{nom,n} = 0 \tag{11}$$

Because of the properties of a cubic spline, there is a linear relation between the function values and the second derivatives at the nodes.[19] In the case of the nominal trajectory, $\boldsymbol{M}_{nom}$ and $\boldsymbol{y}_{nom} = (y_{nom,0}, \ldots, y_{nom,n})^T$ satisfy a linear relation of the form

$$\boldsymbol{B}_{nom} \cdot \boldsymbol{M}_{nom} = \boldsymbol{C}_{nom} \cdot \boldsymbol{y}_{nom} \tag{12}$$

The matrices $\boldsymbol{B}_{nom}$ and $\boldsymbol{C}_{nom}$ may be taken from standard literature on numerical mathematics[19]; they only depend on partition (8). $\boldsymbol{B}_{nom}$ is a tridiagonal, symmetric, positive definite matrix. Therefore, $\boldsymbol{M}_{nom}$ is uniquely determined by Eq. (12) and is assumed to be known in the sequel. Here, $\boldsymbol{y}_{nom}$ and $\boldsymbol{M}_{nom}$ provide the complete information to set up the spline function $f_{nom}(e)$.

For $e \in [e_j, e_{j+1}]$, the nominal trajectory $f_{nom}(e)$ is a cubic polynomial of the form

$$f_{nom}(e) = a_{nom,j} + b_{nom,j}(e - e_j) + c_{nom,j}(e - e_j)^2 + d_{nom,j}(e - e_j)^3 \tag{13}$$

with coefficients depending on $\boldsymbol{y}_{nom}$ and $\boldsymbol{M}_{nom}$:

$$a_{nom,j} = y_{nom,j}, \qquad c_{nom,j} = \frac{M_{nom,j}}{2}$$

$$b_{nom,j} = \frac{y_{nom,j+1} - y_{nom,j}}{h_{j+1}} - \frac{2 \cdot M_{nom,j+1} + M_{nom,j}}{6} \cdot h_{j+1}$$

$$d_{nom,j} = \frac{M_{nom,j+1} - M_{nom,j}}{6 \cdot h_{j+1}} \tag{14}$$

with $h_{j+1} = e_{j+1} - e_j$.

The spline function $f_{ref}(e)$ is set up in a similar way. Just replace the $()_{nom}$ variables by the analogous $()_{ref}$ variables in Eqs. (13) and (14).

The spline function $f_{ref}(e)$ is characterized by an equation system similar to Eq. (12). It is more complicated due to the boundary conditions 1–3 of optimization problem (7). Conditions 1 and 2 determine the function values at the bounds:

$$y_{ref,0} = f_{ref}(e_0), \qquad y_{ref,n} = f_{ref}(e_n) \tag{15}$$

with given data $y_{ref,0}$ and $y_{ref,n}$. Because of the bounds (15), the remaining unknowns are the interior values,

$$\bar{\boldsymbol{y}}_{ref} = (y_{ref,1}, \ldots, y_{ref,n-1})^T$$

The natural spline conditions (11) are replaced as follows. Item 1 in the preceding section specifies the slope at e_n:

$$y'_{\mathrm{ref},n} = f'_{\mathrm{ref}}(e_n) \tag{16}$$

with $y'_{\mathrm{ref},n}$ given. Condition 3 refers to the range matching condition (4). Expressed with $f_{\mathrm{ref}}(e)$, it becomes

$$s = \int_{e_0}^{e_n} f_{\mathrm{ref}}(e)\,\mathrm{d}e \tag{17}$$

Because $f_{\mathrm{ref}}(e)$ is linear in $\boldsymbol{y}_{\mathrm{ref}}$ and $\boldsymbol{M}_{\mathrm{ref}}$ [see Eqs. (13) and (14)], boundary conditions (16) and (17) are linear in $\boldsymbol{y}_{\mathrm{ref}}$ and $\boldsymbol{M}_{\mathrm{ref}}$, too. Together with the standard interpolation conditions in Ref. 19 they constitute a linear relation of the form

$$\boldsymbol{B}_{\mathrm{ref}} \cdot \boldsymbol{M}_{\mathrm{ref}} = \boldsymbol{C}_{\mathrm{ref}} \cdot \bar{\boldsymbol{y}}_{\mathrm{ref}} + \boldsymbol{D}_{\mathrm{ref}} \cdot \boldsymbol{z}_{\mathrm{ref}} \tag{18}$$

where $\boldsymbol{z}_{\mathrm{ref}}$ contains the given boundary values:

$$\boldsymbol{z}_{\mathrm{ref}} = (y_{\mathrm{ref},0},\, y_{\mathrm{ref},n},\, y'_{\mathrm{ref},n},\, s)^T \tag{19}$$

The matrices $\boldsymbol{B}_{\mathrm{ref}}$, $\boldsymbol{C}_{\mathrm{ref}}$, and $\boldsymbol{D}_{\mathrm{ref}}$ only depend on partition (8) and, therefore, are known in advance. $\boldsymbol{B}_{\mathrm{ref}}$ is a regular matrix, but not a symmetric one.

D. Computation of the Reference Trajectory

The reference trajectory is the solution of optimization problem (7) with constraints 1–3. With the spline modeling in the preceding section, problem (7) reduces to the following nonlinear program: Minimize objective function (7) with respect to the parameters $\boldsymbol{M}_{\mathrm{ref}}$ and $\bar{\boldsymbol{y}}_{\mathrm{ref}}$ subject to equality constraint (18).

The weighting function $w(e)$ in problem (7) is defined as a piecewise constant function:

$$w(e) = w_{j+1} = f_{\mathrm{nom}}(e_j)^2, \qquad e_j \le e < e_{j+1} \tag{20}$$

Hence, the relative deviation from the nominal trajectory is integrated in Eqs. (6) and (7). Because of Eq. (20), performance index (7) can be written as

$$I[f_{\mathrm{ref}}] = \left\{ \sum_{j=0}^{n-1} \frac{1}{w_{j+1}} \cdot \int_{e_j}^{e_{j+1}} [f_{\mathrm{ref}}(e) - f_{\mathrm{nom}}(e)]^2\,\mathrm{d}e \right\} + \frac{1}{2} \cdot \Delta \boldsymbol{M}^T \boldsymbol{C} \Delta \boldsymbol{M} \tag{21}$$

where $f_{\mathrm{ref}}(e)$ is linear in $\boldsymbol{M}_{\mathrm{ref}}$ and $\bar{\boldsymbol{y}}_{\mathrm{ref}}$ [see Eqs. (13) and (14)]. Therefore, objective function (21) is quadratic in $\boldsymbol{M}_{\mathrm{ref}}$ and $\bar{\boldsymbol{y}}_{\mathrm{ref}}$. When $\boldsymbol{M}_{\mathrm{ref}}$ is eliminated with Eq. (18), objective function (21) becomes a quadratic function in $\bar{\boldsymbol{y}}_{\mathrm{ref}}$ alone:

$$I[f_{\mathrm{ref}}] = F(\bar{\boldsymbol{y}}_{\mathrm{ref}}) = \tfrac{1}{2} \cdot \bar{\boldsymbol{y}}_{\mathrm{ref}}^T \cdot \boldsymbol{A} \cdot \bar{\boldsymbol{y}}_{\mathrm{ref}} + \boldsymbol{u}^T \cdot \bar{y}_{\mathrm{ref}} + v \tag{22}$$

The quantities $\boldsymbol{A}$, $\boldsymbol{u}$, and v are known in advance because they only depend on partition (8), the weighting factors (20), and the boundary values (19).

The minimum of function (22) with respect to $\bar{\boldsymbol{y}}_{\mathrm{ref}}$ is easily identified by setting $\nabla F = 0$:

$$\nabla F = \boldsymbol{A} \cdot \bar{\boldsymbol{y}}_{\mathrm{ref}} + \boldsymbol{u} = 0 \Rightarrow \bar{\boldsymbol{y}}_{\mathrm{ref}} = -\boldsymbol{A}^{-1} \cdot \boldsymbol{u} \tag{23}$$

Because performance index (7) is an integral over a squared function, it is positive. Therefore, matrix $\boldsymbol{A}$ will be positive definite as well. Hence, $\boldsymbol{A}$ can be inverted, and the optimal solution is unique. With $\bar{\boldsymbol{y}}_{\mathrm{ref}}$ obtained, the second derivatives $\boldsymbol{M}_{\mathrm{ref}}$ can be computed from Eq. (18). This completes the definition of the reference trajectory in the form of Eqs. (13) and (14).

As outlined in Sec. III.B. path constraints would pose upper and lower limits on $f_{\mathrm{ref}}(e)$ and, hence, on the discrete representation $\bar{\boldsymbol{y}}_{\mathrm{ref}}$. This would change the unconstrained quadratic program (22) to a constrained one with constraints of the form

$$\bar{\boldsymbol{y}}_{\mathrm{ref,min}} \le \bar{\boldsymbol{y}}_{\mathrm{ref}} \le \bar{\boldsymbol{y}}_{\mathrm{ref,max}}$$

This extension would be similar to Ref. 3.

The present guidance design essentially follows the concept of Roenneke,[10] who provides the variational problem for the reference trajectory stated in Sec. III.B. Roenneke[10] also introduces the cubic spline modeling of the weight-to-drag history (5) of the reference trajectory. The present approach and Roenneke[10] agree up to this point, but differ in the numerical solution of the variational problem. Roenneke[10] treats both the abscissas and the function values of the spline as optimizable parameters. This leads to a nonlinear program, which is solved iteratively. Real-time integration is used to evaluate a performance index of type (6). Optimizable nodes on the energy axis have the favorable effect that the curvature properties of the reference trajectory change uniformly from one update to the next. The entry trajectory can be modeled as a spline with only two sections and one intermediate node to be optimized.[10] In the present guidance scheme, partition (8) is fixed relative to the bounds of the energy interval; this is the essential difference with Ref. 10. The appeal of the presented discretization is that the variational problem reduces to an unconstrained quadratic program in the remaining unknowns. The solution is determined by a linear equation system; there is no iterative procedure with an inevitable convergence risk. The drawback is that the curvature of the reference trajectory develops somewhat irregularly on the updates. An additional penalty term on the curvature is necessary to suppress undesired oscillations.

E. Entry Phases

Some factors limit the application of the guidance algorithm.

1) The guidance algorithm depends on the drag measurement. At the entry interface, the bias of the accelerometer (used to measure the drag deceleration) is larger than the actual deceleration. The guidance is activated as soon as the drag deceleration has reached a value 10 times the bias. For the assumed measurement device, the minimum drag deceleration is 0.03 m/s^2.

2) According to Eq. (5), the reference trajectory is defined as an energy-dependent weight-to-drag ratio. At the entry interface, the weight-to-drag ratio is of the order of 1000 because of the small drag, and it decreases to the order of unity thereafter. When the guidance is initiated at $D/m = 0.03$ m/s^2, the weight-to-drag ratio still is 333. Because of the well-known overshoot property of splines, it does not make sense to interpolate a set of data where the first function value is of the order of 1000 and the other values are of the order of unity. Apart from just overshooting, the weight-to-drag ratio could even become negative, which is physically impossible.

3) As the distance to the target shrinks to zero, the curvature of the reference trajectory increases because the reference trajectory tries to match the reference range with the range-to-go. As a result, there could be saturation of the commanded bank angle, which means physically that the commanded bank angle would be either 0 or ± 180 deg.

To account for all of these effects the following phase structure is introduced.

1) Phase 1: As long as the drag deceleration is below 0.03 m/s^2, the commanded bank angle is set to 0 deg. This agrees with the bank angle of the nominal trajectory near the entry interface.

2) Phase 2: As soon as the drag deceleration has exceeded 0.03 m/s^2, guidance is initiated. However, to avoid the numerical problems described earlier, the nominal trajectory is represented as the drag profile $D_{\mathrm{nom}}(e)$ and tracked until the weight-to-drag ratio has dropped to a value of one.

3) Phase 3: As soon as the weight-to-drag ratio is smaller than one, the guidance concept presented earlier applies to its full extent, including the update of the reference trajectory at intervals of 30 s.

4) Phase 4: Finally, as soon as specific energy is less than 500 km, the update of the reference trajectory is terminated, and the last reference trajectory is tracked. Later, as soon as velocity drops below 1000 m/s, the commanded bank angle is set to 0 deg, to let the capsule enter the parafoil phase with a lift-up attitude.

The switching criteria are checked every 30 s. In phase 3, these instants coincide with the reference trajectory updates.

IV. Simulation Results in Six Degrees of Freedom

A. Simulation Model

Discrete-time simulations with a high-fidelity simulation program[14,15] were carried out to validate the guidance algorithm. The attitude command of the guidance serves as input to the attitude controller.[17] The drag tracking controller is called each second; the sampling period of the attitude control is 0.1 s. The attitude controller generates a torque command that is converted into thruster commands. The thruster commands are generated with pulse-amplitude modulation instead of pulse-width modulation. The result is a constant, intermediate thrust level over the whole 0.1-s sample period. The intermediate value may be regarded as the mean value of an appropriate pulse sequence.

The desired landing site is Captieux, France (44.4° N, 0.4° W). To provide enough range in the parafoil phase, the atmospheric guidance does not aim at Captieux itself, but rather at an artificial target, which is shifted backward in flight direction about 15 km. The simulation ends as soon as either the final velocity ($V = 450$ m/s) or the final altitude ($h = 25$ km) is reached. The results presented are obtained with "ideal navigation," that is, there is no difference between the actual and measured values.

B. Nominal and Perturbed Cases

To test the robustness of the guidance algorithm, some perturbations of the nominal scenario have been simulated as well. Five cases are presented. Case 1 is the simulation of the nominal mission, which starts at the initial conditions of the ASTOS optimization (Table 2). These initial conditions also apply to case 2 with perturbed aerodynamic coefficients. The perturbations consist of a 10% decrease of $|c_z|$ and a 10% increase of $|c_x|$. Because of the negative angle of attack, this results in a higher L/D ratio. For Mach numbers greater than 10, the gain in L/D is about 14% from 0.383 to 0.437.

Possible ΔV errors of the tangential deorbit impulse are assumed to be limited to ± 2 m/s. Case 3 belongs to the lower limit $\Delta V = -2$ m/s, and case 4 is the entry flight for $\Delta V = +2$ m/s. Table 2 presents the entry conditions for all cases. Velocity, flight-path angle, and heading angle refer to the Earth relative velocity vector. The assumption is that a ΔV variation mainly causes an in-plane error, which does not affect the heading. However, the ΔV variation does change both velocity and flight-path angle at the entry interface at 120-km altitude. For the variation $\Delta V = +2$ m/s, the range-to-go increases about 170 km at the entry interface. The variation $\Delta V = -2$ m/s has the opposite effect.

Case 5 is an example with perturbed air density with a standard deviation $\sigma_z = 30\%$ where σ_z refers to the relative deviation from standard atmosphere. This is accomplished by multiplying air density everywhere in the equations of motion with the factor $(1 + z)$, where z is a zero-mean, first-order Markov process with the standard deviation σ_z:

$$\rho \rightarrow \rho \cdot (1+z), \qquad E(z) = 0, \qquad E(z^2) = \mathrm{Var}(z) = \sigma_z^2 = 0.09$$

To this end, the simulation model is augmented with the differential equation,

$$\dot{z} = -(z/T) + w, \qquad z(0) = 0$$

where w is a white noise input with the constant power spectrum $q > 0$. Note that $z(t)$ is an exponentially correlated random variable.[20] The correlation between z values at two different instants t_1 and t_2 is given by

$$(q \cdot T/2) \cdot \exp(-|t_1 - t_2|/T)$$

The correlation time T is set to 250 s. The power spectrum q is determined by the relation

$$\sigma_z^2 = (q \cdot T)/2 = 0.09$$

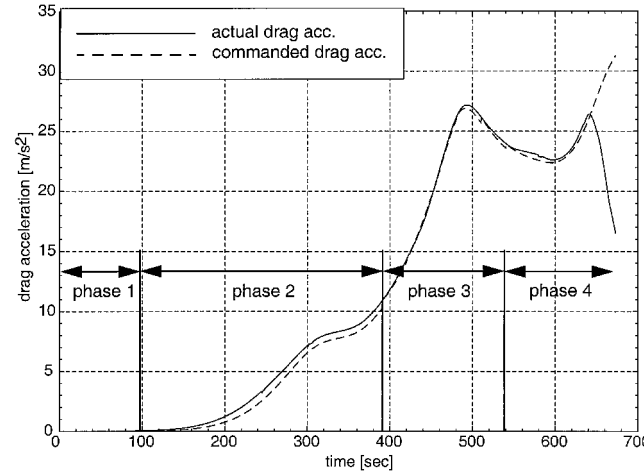

Fig. 2 Actual and commanded drag acceleration under nominal conditions.

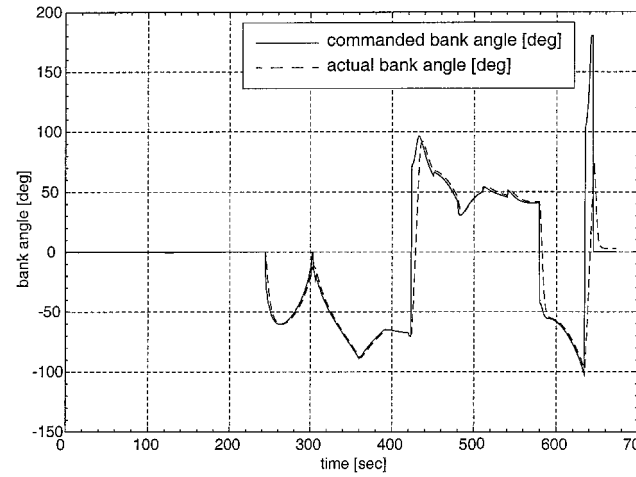

Fig. 3 Actual and commanded bank angle under nominal conditions.

C. Results

Figure 2 shows the drag command and the drag response of the guided vehicle in a six-degree-of-freedom simulation under nominal conditions. During phase 2 up to about 390 s, the drag command is taken from the nominal trajectory. There is a persistent error of about 0.5 m/s^2 in drag tracking. The error is partially due to control saturation indicated by $\mu_{\mathrm{com}} = 0$ until $t = 240$ s (Fig. 3). The bank angle of the nominal trajectory is nearly zero in the first 250 s, which means a lack of control margin. Phase 3 begins at $t \approx 390$ s, with the first update of the reference trajectory. Note that the reference drag profile always starts at the current drag value (Sec. III.B). There are five further updates at time intervals of 30 s. At each update, the drag command is smooth and continuous, as required by the guidance constraints. This also guarantees a smooth bank angle command history and good bank angle tracking (Fig. 3). During phase 3, the vehicle sufficiently tracks the drag command, resulting in a final target miss of 4 km (Table 3). A total of three bank reversals are necessary to achieve sufficient crossrange control. The effect of the bank reversals is hardly visible in the drag history. This was expected because of the low L/D ratio of the vehicle.

The last update of the reference drag profile occurs at $t \approx 540$ s (Fig. 2). This indicates the transition to phase 4, where the reference drag profile remains unchanged. At the end of phase 4, the bank command is set to zero to achieve a lift-up attitude at the beginning of the parafoil phase. The final segment with $\mu_{\mathrm{com}} = 0$ starts at $t \approx 640$ s. It is visible in Fig. 2 at the instant where drag tracking terminates.

Figures 4 and 5 show simulation results for the off-nominal cases in the drag and altitude vs velocity domains, respectively. In case 2,

Table 3 Final data of the simulations

Quantity	Case 1 (nominal)	Case 2 (perturbed aerodynamics)	Case 3 ($\Delta V = -2$ m/s)	Case 4 ($\Delta V = +2$ m/s)	Case 5 (perturbed density)
Final declination, deg	44.412	44.475	44.475	44.673	44.408
Final longitude, deg	−0.561	−0.667	−0.610	−0.682	−0.556
Final altitude, km	25.9	25.3	25.3	25.3	25.4
Final velocity, m/s	464	643	596	550	675
Final flight-path angle, deg	−18	−26	−23	−23	−19
Final heading angle, deg	122	94	122	136	127
Miss distance, km	4.0	7.8	4.1	26.5	4.9

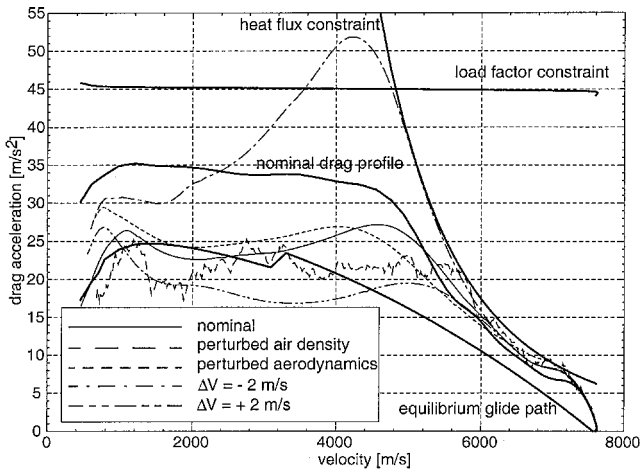

Fig. 4 Drag acceleration vs velocity for nominal and perturbed cases.

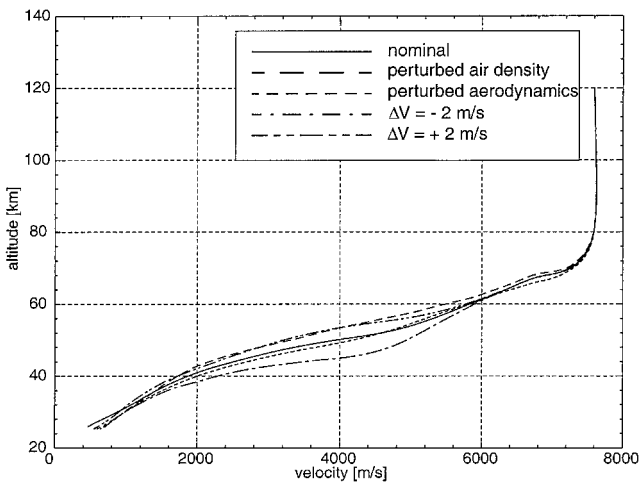

Fig. 5 Altitude vs velocity for nominal and perturbed cases.

the capsule flies a trajectory that is close to the nominal case 1 in spite of the variation of the aerodynamics. In case 3, the effect of −2-m/s offset on the nominal deorbit impulse is a shorter range to the target at entry interface (about 170 km). Moreover, the flight path at the entry interface is about 0.05 deg flatter than in the nominal case 1. The range error is compensated by a shift of the commanded drag trajectory to higher drag levels. The equivalent shift in altitude can be seen in Fig. 5. Case 4 represents the opposite of case 3. If the nominal deorbit impulse is increased about 2 m/s, the distance to the target at entry interface becomes about 170 km longer compared to nominal conditions. The entry flight-path angle is about 0.04 deg steeper. The range error is compensated for by a shift of the drag command to lower drag levels. The lifting capability of the vehicle is not sufficient to maintain the corresponding altitude throughout the flight. The drag is distinctly below the equilibrium glide path for a large velocity interval. There is an interval with $\mu_{\text{com}} = 0$ of about 100-s duration in phase 4. During this period, the capsule fails to track the commanded drag. This explains the miss distance of 26.5 km at the end.

In all cases, the vehicle has difficulties in tracking the nominal drag profile precisely in phase 2 (Fig. 2 for the nominal case 1). The actual drag is always higher than the nominal one for $V > 6$ km/s (Fig. 4). The undesired deceleration in the high-speed regime causes a range error, which is successfully corrected by a reduction of the nominal drag level in the remaining flight (cases 1, 2, 4, and 5). This is most obvious in case 5. The random perturbation of the air density is such that the flight is close to the heat flux limit up to $V = 5.6$ km/s. Also, the intensity of the perturbation is beyond realistic magnitude. The results call for a refinement of the nominal drag profile. A drag level above the centerline of the corridor might improve the guidance. Sufficient control margin throughout the whole trajectory is mandatory.

Figure 4 shows that the path constraints may be violated in off-nominal situations. If the range-to-go is distinctly shorter than the nominal one (case 3) the load factor exceeds its limit. In the opposite case (case 4) the corrected drag level is below the equilibrium glide limit. This is more critical in terms of landing accuracy because controllability may be lost. In both cases, however, the modified drag profile precisely compensates the range error.

V. Conclusions

The present paper describes an update scheme for reference drag profiles within an entry guidance algorithm. The reference drag profile is the solution of a variational problem. The objective is to cover the required range to the target along a trajectory that is as close as possible to a precalculated path (nominal trajectory). The numerical discretization reduces the variational problem to an unconstrained quadratic program, the coefficients of which can be evaluated in closed form. This helps to reduce CPU time and facilitates real-time application. Because of the use of cubic splines, a penalty term on the curvature is required to obtain a smooth profile. Smoothing would also be enhanced by movable discretization grid points. This, however, would create a general nonquadratic optimization problem with all implications for onboard calculation.

The update scheme does not explicitly account for path constraints such as heating, load factor, or dynamic pressure constraints. It is supposed that the nominal trajectory provides sufficient margin to the constraints. Path constraints could be introduced as bounds on the unknown parameters of the quadratic program.

The optimized drag profile starts at the current state of the vehicle. Thus, a sudden drag error on tracking the profile is avoided. This is a refinement over the shuttle guidance, for instance. In the presented simulations, perturbations on the deorbit impulse, the aerodynamic coefficients, and air density are successfully compensated.

In the present scheme, range correction begins as soon as drag acceleration exceeds gravitational acceleration. A failure to track the nominal drag profile in the preceding flight phase causes a range error, which must be compensated by a significant variation of the nominal drag profile on the remaining flight. Future work will address improvement of the guidance immediately after the entry interface. In particular, sufficient control margin is necessary throughout the nominal trajectory.

The versatility of the approach, for example, its application to planetary entry and return missions to Earth, and its robustness to varying initial and boundary conditions are subjects of future studies.

Acknowledgment

This research was supported by the European Space Research and Technology Centre, Noordwijk, The Netherlands, as part of the "Autonomous GNC for Atmospheric Entry and Precision Landing of Small Capsules" study.

References

[1]Harpold, J. C., and Graves, C. A., "Shuttle Entry Guidance," *Journal of the Astronautical Sciences*, Vol. 27, No. 3, 1979, pp. 239–268.

[2]Hanson, J. M., Coughlin, D. J., Dukeman, G. A., Mulqueen, J. A., and McCarter, J. W., "Ascent, Transition, Entry, and Abort Guidance Algorithm Design for the X-33 Vehicle," AIAA Paper 98-4409, Aug. 1998.

[3]Lu, P., "Entry Guidance and Trajectory Control for Reusable Launch Vehicle," *Journal of Guidance, Control, and Dynamics*, Vol. 20, No. 1, 1997, pp. 143–149.

[4]Lu, P., and Hanson, J. M., "Entry Guidance for the X-33 Vehicle," *Journal of Spacecraft and Rockets*, Vol. 35, No. 3, 1998, pp. 342–349.

[5]Ishizuka, K., Shimura, K., and Ishimoto, S., "A Re-Entry Guidance Law Employing Simple Real-Time Integration," AIAA Paper 98-4329, Aug. 1998.

[6]Mease, K. D., Teufel, P., Schönenberger, H., Chen, D.T., and Bharadwaj, S., "Re-Entry Trajectory Planning for a Reusable Launch Vehicle," AIAA Paper 99-4160, Aug. 1999.

[7]Schöttle, U. M., Burkhardt, J., and Zimmermann, F., "Optimal Flight Control of a Re-Entry Capsule with Consideration of Mission Constraints," AIAA Paper 97-3659, Aug. 1997.

[8]Zimmerman, C., Dukeman, G., and Hanson, J., "An Automated Method to Compute Orbital Re-Entry Trajectories with Heating Constraints," AIAA Paper 2002-4454, Aug. 2002.

[9]Dukeman, G. A., "Profile-Following Entry Guidance Using Linear Quadratic Regulator Theory," AIAA Paper 2002-4457, Aug. 2002.

[10]Roenneke, A. J., "Adaptive On-Board Guidance for Entry Vehicles," AIAA Paper 2001-4048, Aug. 2001.

[11]Roenneke, A. J., and Well, K. H., "Nonlinear Drag-Tracking Control Applied to Optimal Low-Lift Re-Entry Guidance," AIAA Paper 96-3698, July 1996.

[12]Mease, K. D., and Kremer, J. P., "Shuttle Entry Guidance Revisited," AIAA Paper 92-4450, Aug. 1992.

[13]Markl, A., Wiegand, A., Gath, P., Well, K. H., and Paus, P., "ASTOS—Re-Entry Application Manual," Inst. of Flight Mechanics and Control, Stuttgart Univ., Stuttgart, Germany, Jan. 2003.

[14]Klotz, H., Markus, M., Grimm, W., and Strandmoe, S. E., "Guidance and Control for Autonomous Re-Entry and Precision Landing of a Small Capsule," *Proceedings of the 4th ESA International Conference on Spacecraft Guidance, Navigation, and Control Systems*, European Space Research and Technology Centre, Noordwijk, The Netherlands, 1999.

[15]Klotz, H., Starke, J., Frapard, B., Champetier, C., Grimm, W., and Strandmoe, S. E., "Guidance, Navigation, and Control for Autonomous Re-Entry and Precision Landing of Future Small Capsules," *Proceedings of the AAAF International Symposium on Atmospheric Re-Entry Vehicles and Systems*, Association Aéronautique et Astronautique de France (AAAF), Verneuil, France, 1999.

[16]*CapRee Study Reference Design Concept*, Document CAP-TN-002-98-DA, ESA/European Space Research and Technology Centre, Noordwijk, The Netherlands, 1999.

[17]Roenneke, A. J., and Well, K. H., "Nonlinear Flight Control for a High-Lift Re-Entry Vehicle," AIAA Paper 95-3370, Aug. 1995.

[18]Roenneke, A. J., and Markl, A., "Reentry Control to a Drag-vs-Energy Profile," *Journal of Guidance, Control, and Dynamics*, Vol. 17, No. 5, 1994, pp. 916–920.

[19]Stoer, J., and Bulirsch, R., *Introduction to Numerical Analysis*, Springer, New York, 1980.

[20]Friedland, B., "Random Processes," *Control System Design—An Introduction to State-Space Methods*, 2nd Printing, McGraw–Hill, New York, 1987, pp. 378–403.